Supporting Information

Meng et al. 10.1073/pnas.0913759107

SI Materials and Methods

Expression Analysis. One microgram total RNA, isolated using TRIzol reagent (Invitrogen) and purified with DNase treatment (Promega), was reverse transcribed into cDNA with random primers using M-MLV reverse transcriptase (Promega) in a 25-μL volume. cDNA (0.5 μL) or total RNA (0.5 μg) (no RT as DNA contamination control) was used directly as PCR template. DNA Engine Opticon 1 (MJ Research) was used for real-time quantitative PCR with 18S rRNA as internal control. Relative quantitative PCR results were analyzed using the $2^{-\Delta\Delta C}{}_T$ method (1).

Screen for T-DNA Insertion Mutants. Primers from the T-DNA left border LB1 and gene-specific primers (Table S2) were used to screen for the T-DNA insertion with PCR; results were confirmed by sequencing. Homozygous mutants for the T-DNA insertion were analyzed using RT-PCR. For the Trx *h*9 mutant screen, 22% of the T_3 plants in the Salk_08660 line were heterozygous for the T-DNA insertion. No plants homozygous for the T-DNA insertion were found among T_3 plants; 2.83% of the T_4 progeny from two T_3 heterozygous parental plants of Salk_08660 line were found to be homozygous for the T-DNA insertion and for the null loss-of-function mutants of Trx *h*9. In the Trx *p* mutation screen, 28.6% of the T_3 plants in Salk_028162 were heterozygous for the T-DNA insertion; no homozygous T-DNA insertion plants were found among the T_3 plants; 3.7% of T_4 progeny from a T_3 heterozygous parental plant of Salk_028162 appeared to be as homozygous and null knockout mutants of Trx *p*. The non-Mendelian segregation ratios (ca 3% vs. 25%) for both the *trx h*9 and *trx p* mutants suggest that the mutations in both cases have remarkably lowered the viability and passing of the inactive allele from parents to offspring.

Transmission Electron Microscopy. Transmission electron microscopy images were obtained following the protocols indicated for use of an FEI Tecnai 12 120-kV transmission electron microscope (http://em-lab.berkeley.edu/EML/protocols.php).

Chlorophyll Analysis. HPLC analysis of chlorophylls was done as described (2).

Protein Extraction and Western Blot Analysis. Soluble proteins were extracted from 7-day-old homozygous T_2 transgenic *Arabidopsis* seedlings (3). Insoluble proteins present in the pellet were re-extracted with a buffer (50 mM Tris-HCl, 1.0% SDS, 2% β-mercaptoethanol, pH 8.0) by shaking at room temperature for 1 h. The western blot analysis of Trx-GFP was performed with a GFP antibody (Santa Cruz Biotechnology) as described (3).

Trx *h*9 May Dock via Interaction of N-Terminal Cys^4 with Catalytic Cys^{57}. Using PtTrx *h*4 and other close homologs as templates for comparative modeling, we determined a predicted 3D structure for Trx *h*9. Unfortunately, amino acids 1–23, representing the entire N-terminal extension of PtTrx*h*4, could not be located in the 3D structure due to the weak electron density of signals from this region (4). In view of this structural incompleteness, we proceeded to model Trx *h*9 by applying I-TASSER simulation. With this approach, the missing portions of Trx h9 were predicted, leading to a statistically reliable complete 3D structural model. C scores (from –5.0 to 2.0) and TM scores (from 0.0 and 1.0) measure the quality of a predicted model. C scores and TM scores for the models are, respectively, 0.03 and 0.72 for Trx *h*9; 0.03 and 0.69 for Trx *h*9G2A; –0.3 and 0.68 for Trx *h*9C4W; and –0.11 and 0.70 for Trx *h*9C4S. Each model was above the cutoff, that is, C score = –1.5, TM score = 0.5, and thus statistically valid (5).

Docking Modeling of Trx*h*9 Using a Two-Step Procedure of PatchDock and FireDock Services. To explore docking properties of Trx *h*9 with NTR and Grx, we predicted interaction models of Trx *h*9 and AtNTRB (PDB ID code 1vdc), and of Trx *h*9 and Grx. Two Grxs from poplar, PtGrxC1 (PDB ID code 1z7p) and PtGrxS12 (PDB ID code 3fz9), were used. A two-step procedure was used to study the docking models, starting with rigid-body docking by the PatchDock web server (6). These results were redirected for refinement and scoring by the FireDock server (7).

SI Results and Discussion

Grx, Not NTR, Fits in the Potential Binding Pocket of Trx *h*9. Computational docking analysis of Trx *h*9 revealed that Trx *h*9 seemed not to interact with NADP-thioredoxin reductase (NTR), like other *h*-type Trxs (Fig. S6 *A* vs. *B*). Rather, its predicted structure indicated that it was preferentially reduced by the GSH/Grx system, as for the poplar ortholog of Trx *h*9, PtTrx*h*4 (8). NTR (AtNTRB) was too large to fit the Trx *h*9 binding pocket, which did, however, accommodate PtGrxC1 (Fig. S6 *D* and *E*). Specifically, the N-terminal arm of Trx *h*9 appeared to interfere with NTR (AtNTRB) (Fig. S6*A*), but wrapped around Grx (PtGrxC1), yielding a tight and stable complex (Fig. S6 *D* and *E*). Predicted specificity of Trx *h*9 was supported by the observation that Trx *h*1, which is reduced by NTR (9), fits perfectly with the enzyme (AtNTRB) (Fig. S6*B*) but not with Grx (PtGrxC1) (Fig. S6 *B* vs. *C*).

In contrast to its interference with binding Trx *h*9 to the plasma membrane (Fig. 3 *E*–*H*), mutation of Gly^2, that is, Trx *h*9G2A, had no effect on the predicted interaction of Trx *h*9 with Grx (PtGrxC1) (Fig. S6 *F* and *G*). However, mutation of Cys^4 to tryptophan (Trx *h*9C4W) seemingly abolished this ability (Fig. S6 *H* and *I*). Although the main body of the tryptophan mutant Trx *h*9C4W could interact with PtGrxC1, the N-terminal extension could not wrap around the partner molecule. A similar effect was seen when Cys^4 was mutated to Ser. When PtGrxS12 was used for docking, a similar result was obtained. The structures suggest that Trx *h*9 links the Grx and Trx systems in redox signaling in *Arabidopsis*, as reported for poplar (4).

1. Livak KJ, Schmittgen TD (2001) Analysis of relative gene expression data using real-time quantitative PCR and the 2(−ΔΔC(T)) method. *Methods* 25:402–408.
2. Müller-Moulé P, Conklin PL, Niyogi KK (2002) Ascorbate deficiency can limit violaxanthin de-epoxidase activity in vivo. *Plant Physiol* 128:970–977.
3. Cho M-J, et al. (1999) Overexpression of thioredoxin *h* leads to enhanced activity of starch debranching enzyme (pullulanase) in barley grain. *Proc Natl Acad Sci USA* 96: 14641–14646.
4. Koh CS, et al. (2008) An atypical catalytic mechanism involving three cysteines of thioredoxin. *J Biol Chem* 283:23062–23072.
5. Zhang Y (2008) I-TASSER server for protein 3D structure prediction. *BMC Bioinformatics* 9:40.
6. Schneidman-Duhovny D, Inbar Y, Nussinov R, Wolfson HJ (2005) PatchDock and SymmDock: Servers for rigid and symmetric docking. *Nucleic Acids Res* 33 (Web Server issue):W363–W367.
7. Mashiach E, Schneidman-Duhovny D, Andrusier N, Nussinov R, Wolfson HJ (2008) FireDock: A web server for fast interaction refinement in molecular docking. *Nucleic Acids Res* 36 (Web Server issue):229–232.
8. Gelhaye E, Rouhier N, Jacquot JP (2003) Evidence for a subgroup of thioredoxin *h* that requires GSH/Grx for its reduction. *FEBS Lett* 555:443–448.
9. Meyer Y, Buchanan BB, Vignols F, Reichheld JP (2009) Thioredoxins and glutaredoxins: Unifying elements in redox biology. *Annu Rev Genet* 43:335–367.
10. Brown DP, Krishnamurthy N, Sjölander K (2007) Automated protein subfamily identification and classification. *PLoS Comput Biol* 3:e160.

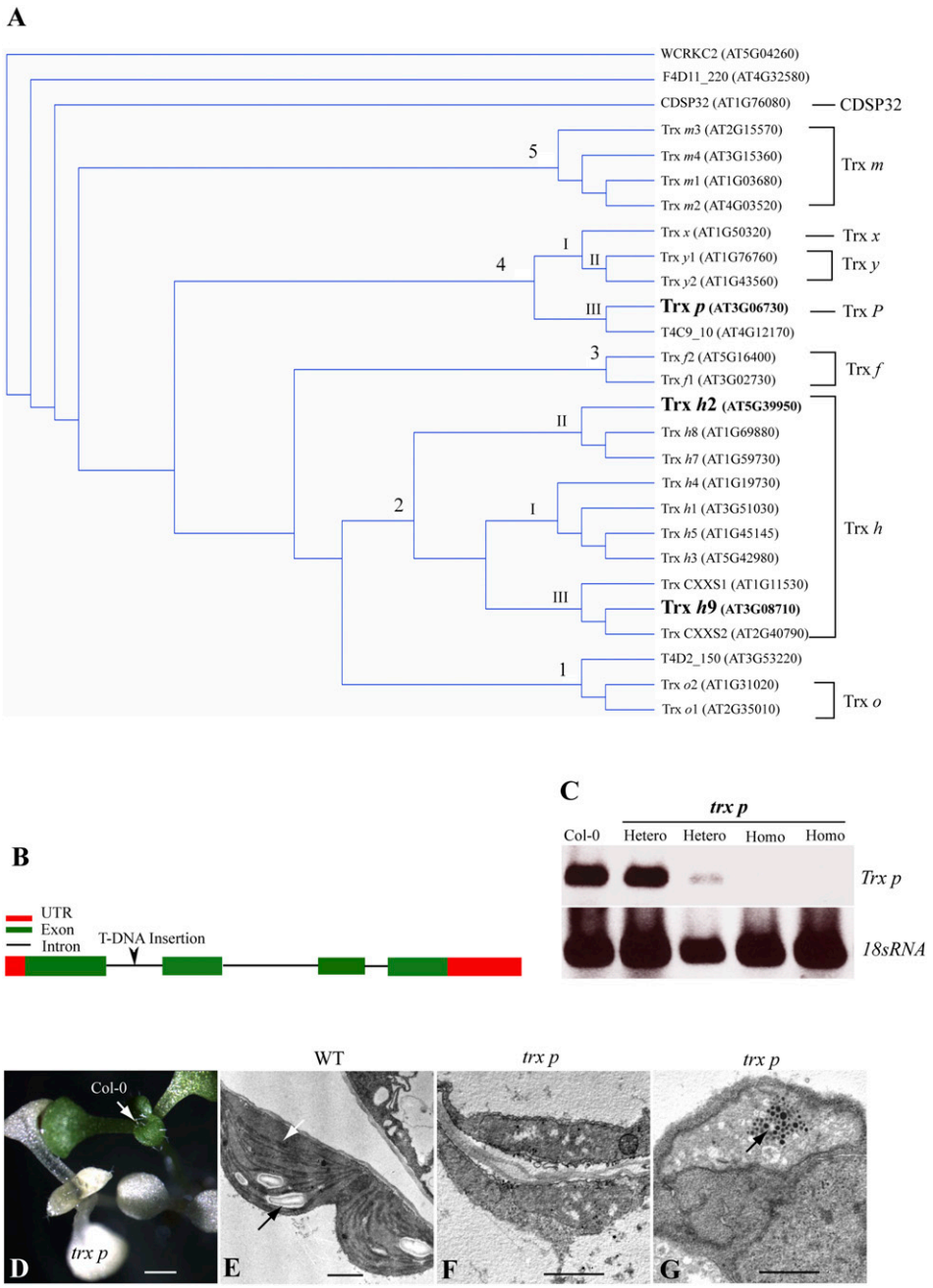

Fig. S1. Subfamily classification of *Arabidopsis* Trxs and loss-of-function analysis of Trx *p*. (*A*) Subfamily classification of Trxs in *Arabidopsis* using SCI-PHY (10) (http://phylogenomics.berkeley.edu/cgi-bin/SCI-PHY/input_SCI-PHY.py). (*B*) Schematic representation of *Trx p* gene structure with a T-DNA insertion in Salk_028162 line. (*C*) RT-PCR analysis of *Trx p* expression in Salk_028162 mutant line, compared to that from WT (Col-0) and heterozygous and homozygous Salk_028162 plants. (*D*–*G*) Phenotypic analysis of the homozygous Salk_028162 mutant plants. (D) Five-day-old *Arabidopsis* seedlings grown on MS plus 1% sucrose. Homozygous mutant plants showed a severe albino phenotype. Arrow points to wild-type *Arabidopsis* (Col-0) plant. (*E*–*G*) Transmission electron micrographs of plastids in 5-day-old wild-type (*E*) and mutant (*F*, *G*) *Arabidopsis* seedlings. White arrow in *E* points to stacked grana; black arrow points to starch granule. [Scale bars, 0.5 cm (*D*), 1 μm (*E*–*G*).]

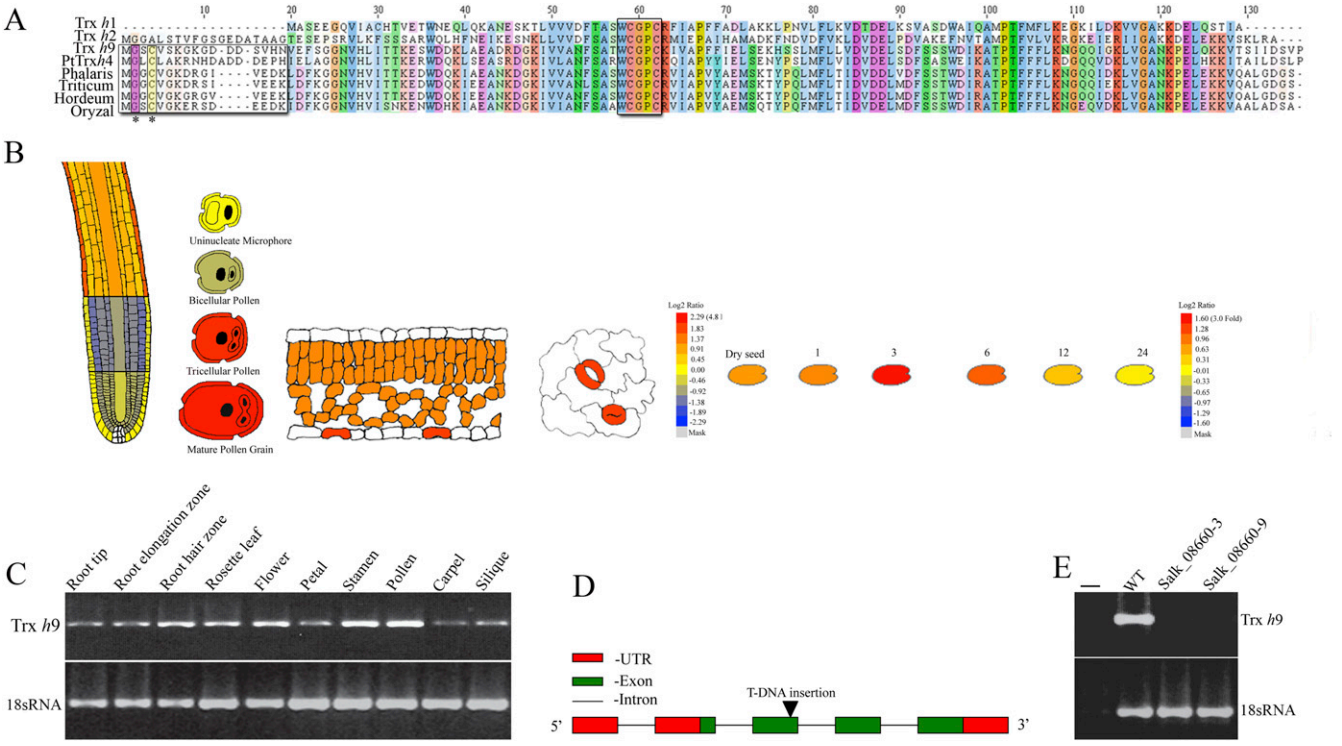

Fig. S2. Protein sequence, gene expression and structure, and loss-of-function analysis of Trx *h*9. (*A*) Protein multiple-sequence alignment of Trx *h*9 and its homologs using ClustalW2. (*B*) Tissue-specific expression of Trx *h*9 in *Arabidopsis* Col-0 plants retrieved from gene expression microarray data through the *Arabidopsis* eFP Browser (http://www.bar.utoronto.ca/efp/cgi-bin/efpWeb.cgi). Intensity of expression of Trx *h*9 is indicated by the color scheme on the right. (*C*) RT-PCR analysis of Trx *h*9 expression in different tissues of wild-type *Arabidopsis* Col-0 plants. (*D*) Schematic representation of *Trx h*9 structure with T-DNA insertion in Salk_08660 line. (*E*) RT-PCR analysis of Trx *h*9 expression in Salk_08660 line: No RT as DNA contamination control. Internal control (bottom panel) used primers for 18S RNA. GenBank accession nos. in *A*: NP_190672 (Trx *h*1), NP_198811 (Trx *h*2), NP_187483 (Trx *h*9), XP_002309192 (PtTRXh4; *Populus trichocarpa*), AAD49233 [thioredoxin-like protein (*Phalaris coerulescens*)], AAN63616 [thioredoxin *h*-like protein (*Hordeum vulgare* subsp. vulgare)], AAN63622 [thioredoxin (*Triticum aestivum*)], NP_001042127 [Os01g0168200, Trx family protein (*Oryza sativa*)]. The classic catalytic site (WCGPC) of Trxs and the N-terminal extensions of Trx *h*9 and its orthologs are indicated by rectangles in *A*. Asterisks denote conserved glycine and cysteine residues at positions 2 and 4, respectively, of the N-terminal extension of Trx *h*9 in *A*.

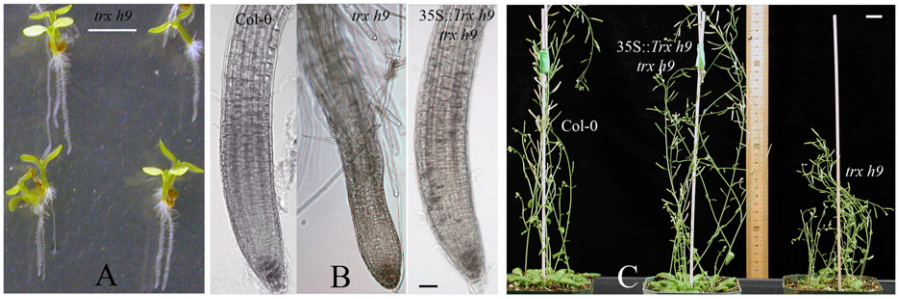

Fig. S3. Phenotypic analysis of *trx h*9 mutation in Salk_08660 plants grown in light. (*A*) Ten-day-old *trx h9* mutant seedlings grown on MS medium without sucrose, showing absence of leaves. (*B*) The root tips of 7-day-old *Arabidopsis* seedlings grown on MS medium plus 1.0% sucrose (left to right: wild-type *Arabidopsis* Col-0 plant, homozygous *trx h*9 mutant, and 35S::*Trx h*9 in *trx h*9 background). (*C*) Eight-week-old *Arabidopsis* plants grown in soil (left to right: wild-type *Arabidopsis* Col-0 plant, 35S::*Trx h*9 in *trx h*9 background, and homozygous *trx h*9 mutant). [Scale bars, 1 cm (*A*), 50 μm (*B*), 2 cm (*C*).]

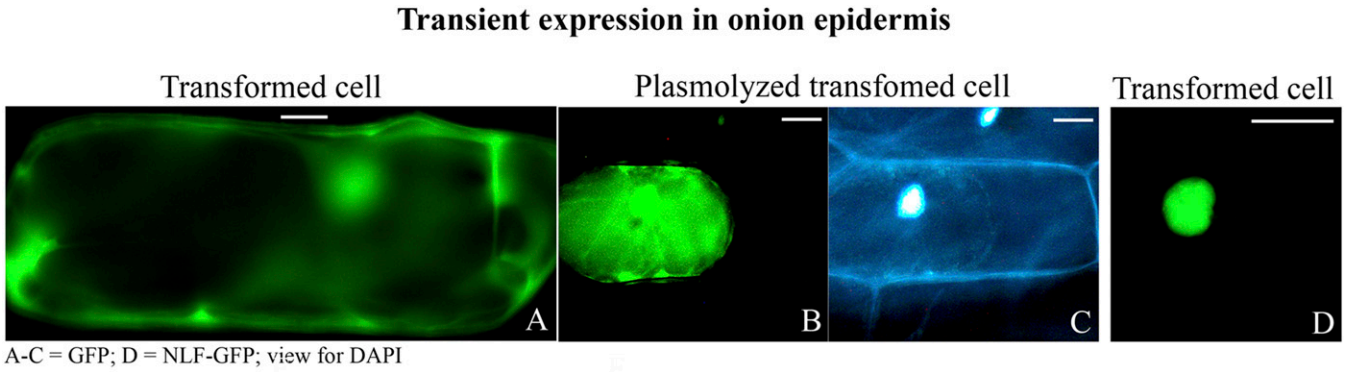

Fig. S4. Confirmation of GFP fusions using transient expression in onion epidermal cells. (*A*–*C*) GFP only. (*D*) NLS-GFP. (*A*, *D*) Nonplasmolyzed, transformed onion epidermal cells. (*B*, *C*) Plasmolyzed, transformed onion epidermal cells. GFP visualized in *B*; DAPI staining visualized in *C*. (Scale bars, 10 μm.)

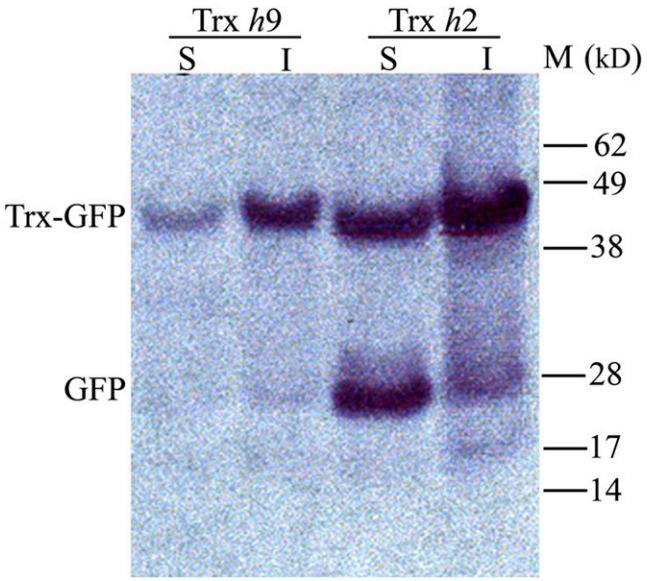

Fig. S5. Western blot analysis of Trx-GFP fusion proteins using a GFP antibody. S and I represent the soluble and insoluble protein portions, respectively. M, SeeBlue Plus2 prestained standards (Invitrogen).

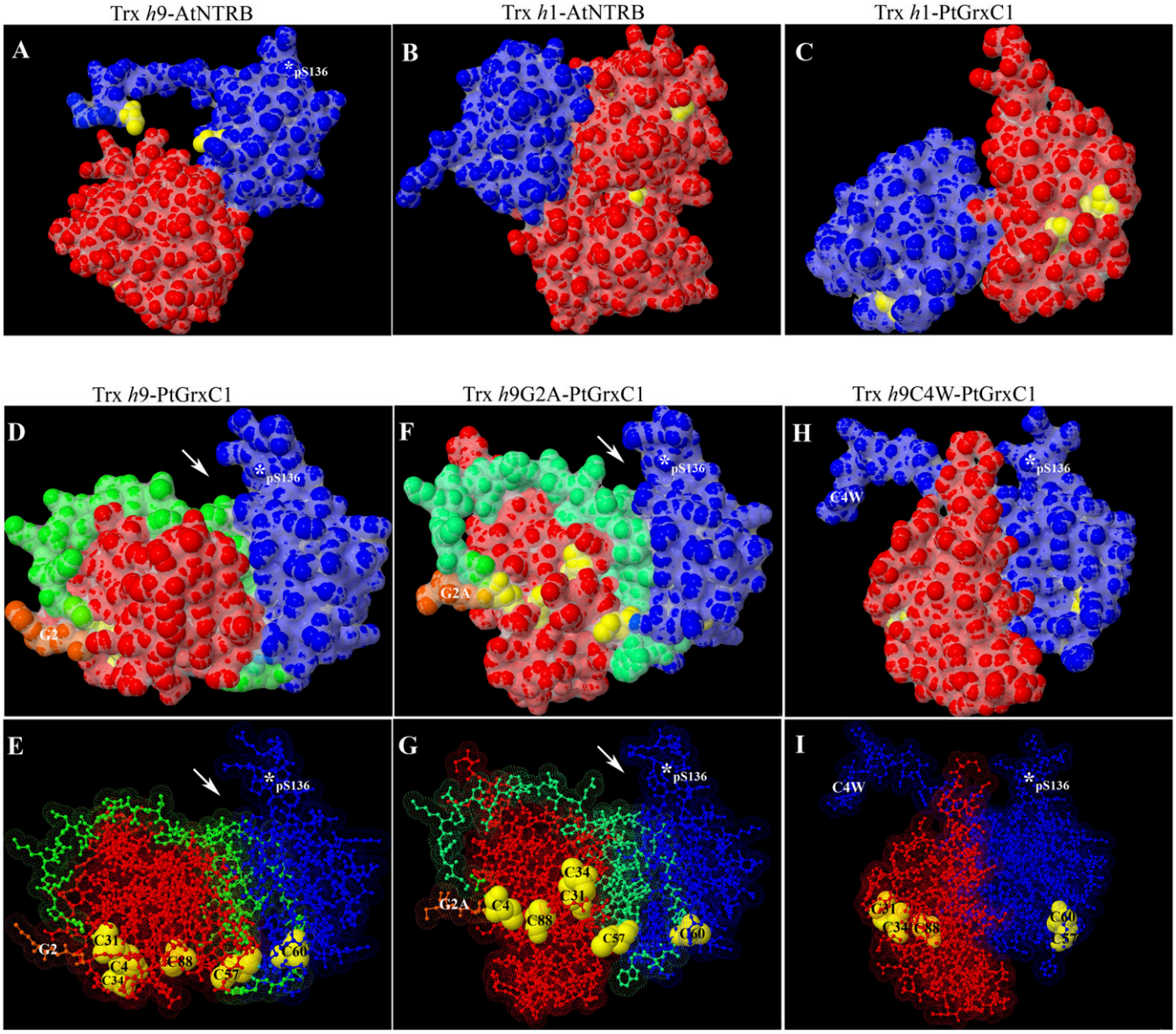

Fig. S6. Docking property analysis of Trx *h*9 and Trx *h*1. (*A*) Docking model of Trx *h*9 with AtNTRB. (*B* and *C*) Docking models of Trx *h*1 (PDB ID code 1XFLA) with AtNTRB (PDB ID code 1vdc) (*B*) and PtGrxC1 (PDB ID code 1z7p) (*C*). (*D* and *E*) Docking model of Trx *h*9 with PtGrxC1. (*F* and *G*) Docking model of Trx *h*9G2A with PtGrxC1. (*H* and *I*) Docking model of Trx *h*94CW with PtGrxC1. Atoms are displayed as 100% of van der Waals with solvent surface (1.4-Å probe) in *A*–*D*, *F*, and *H*. Atoms are displayed as 20% of van der Waals with solvent surface (1.4-Å probe), rendered as discrete dots in *E*, *G*, and *I*. AtNTRB is shown in red in *A* and *B*. Trx *h*9 is shown in blue in *A*, *H*, and *I*, and Trx *h*1 in blue in *B* and *C*. PtGrxC1 is shown in red in *C*–*I*. The main body and N-terminal arm of Trx *h*9 are displayed in blue and green, respectively, in *D*–*G*. Arrows in *D*–*G* point to potential docking sites of proteins. Cysteines are shown in yellow as 100% of van der Waals in *A*–*I* with their numbered amino acid position also indicated in *E*, *G*, and *I*. Asterisks indicate the phosphorylated serine at position 136 (pS136) at the C terminus of Trx *h*9. The Gly^2 mutation to Ala is indicated as G2A, and the Cys^4 mutation to tryptophan (W) as C4W.

Other Supporting Information Files

Table S1 (XLS)
Table S2 (XLS)